Frozen states and order-disorder transition in the dynamics of confined membranes

Thomas Le Goff[1], Paolo Politi[2,3], and Olivier Pierre-Louis[1]
[1] *Institut Lumière Matière, UMR5306 Université Lyon 1-CNRS, Université de Lyon 69622 Villeurbanne, France*
[2] *Istituto dei Sistemi Complessi, Consiglio Nazionale delle Ricerche, Via Madonna del Piano 10, 50019 Sesto Fiorentino, Italy*
[3] *INFN Sezione di Firenze, via G. Sansone 1, 50019 Sesto Fiorentino, Italy.*
(Dated: September 10, 2014)

The adhesion dynamics of a membrane confined between two permeable walls is studied using a two-dimensional hydrodynamic model. The membrane morphology decomposes into adhesion patches on the upper and the lower walls and obeys a nonlinear evolution equation that resembles that of phase separation dynamics, which is known to lead to coarsening, i.e. to the endless growth of the adhesion patches. However, due to the membrane bending rigidity the system evolves towards a frozen state without coarsening. This frozen state exhibits an order-disorder transition when increasing the permeability of the walls.

PACS numbers: 05.45.-a,64.60.-i,87.16.D

arXiv:1409.2525v1 [cond-mat.soft] 8 Sep 2014

I. INTRODUCTION

Two-state continuum models [1, 2], such as the time-dependent Ginzburg-Landau (TDGL) equation or the Cahn-Hilliard (CH) equation have been widely studied as a paradygm of phase transition dynamics in various systems, such as magnetism, liquid-liquid phase separation, or wetting. These models exhibit a phenomenology characterized by their coarsening behavior, i.e. the perpetual increase of the typical lengthscale of the homogeneous zones (where one phase only is present). In this paper, we propose a one-dimensional two-state continuum model inspired by adhesion of confined membranes, which gives rise to a different phenomenology without coarsening and with an order-disorder transition.

Our motivation is to investigate the adhesion dynamics of lipid membranes in biological systems. Lipid membranes are ubiquitous in living organisms. They are the main constituent of the cell membrane [3], and also appear in stacks, e.g. in the stratum corneum of the skin [4–6]. It is therefore crucial to study their physical properties, and especially adhesion, in order to understand their biological functions. Adhesion of membranes on substrates [7–9], may include various physical ingredients, such as e.g. van der Waals attraction and hydration forces [10], ligand-receptor pairs [11, 12], interactions with the cytoskeleton [13], osmotic pressures [14], or entropic interactions [15–17]. In this paper, we do not describe these specific ingredients, and we rather consider an effective adhesion potential, with a potential minimum corresponding to an equilibrium adhesion state close to the substrate[10].

The main goal of our work is to study the consequences of confinement on the nonlinear dynamics of membrane adhesion. In order to mimic confinement within the simplest possible setting, we consider a membrane located between two parallel flat walls. The membrane then experiences a total potential which is the sum of the adhesion potentials of the two substrates. When the distance between the walls is wider than the equilibrium distance of a supported membrane on a single wall, the membrane experiences a double-well potential with a minimum near each wall, as shown in Fig. 1. Such a double-well potential can be found in different instances in biological systems. First, in cell adhesion, this double-well potential could account for the possibility of a membrane to attach to the cytoskeleton inside the cell or to a substrate outside the cell. Moreover, in membrane stacks [14, 17], each membrane may adhere to its neighbors within the stack. Furthermore, double-well potentials are also found to arise in the presence of ligands of two different lengths which enforce two different equilibrium distances in cell-cell adhesion [18]. In addition, they are also observed experimentally in the combined presence of ligands and van der Waals attraction which respectively induce short-range and long-range attractive potentials, and of glycocalyx and other grafted polymers which induce a soft repulsion at intermediate scales [19, 20].

As a consequence of the double-well, the two walls compete for the adhesion of the membrane, which is expected to adhere partially on the upper wall, and partially on the lower wall. At first sight, such a decomposition into adhesion patches might exhibit some similarity with phase separation dynamics [1], the membrane height $h(x,t)$ playing the role of the order parameter. However, in contrast to usual interfaces which are controlled by surface tension, membranes exhibits bending rigidity [21, 22]: the membrane energy density is proportional to the mean curvature squared instead of being proportional to the area. We shall see in the following that this feature leads to a novel phenomenology with frozen states: adhesion patches do not grow and coarsening is absent. From an analysis of the nonlinear steady-states, we argue that these frozen steady-states result from the locking of bending-induced membrane oscillations into each-other.

Our results could have some relevance in a recent debate about the formation and stability of finite-size adhesion domains in cell adhesion. Different studies have suggested the crucial role of the clustering of ligand-receptor

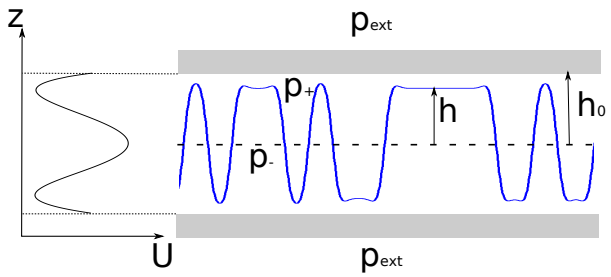

FIG. 1. (Color online) Schematics of a membrane confined between two permeable walls.

pairs [23–25], of the disorder of the environment [13], of the trapping of ligands in membrane partitions [26], or of the active remodeling of the cytoskeleton [27]. We wish to stress that our model where adhesion is driven by a simple distance-dependent free energy potential does not account for the full complexity of specific adhesion in cells, which involves, e.g., the attachement-detachment, diffusion, and interactions of ligand-receptor pairs, and other ingredients mentioned above. However, our results indicate a reduced set of physical ingredients which allows one to obtain finite adhesion patches: bending rigidity and confinement.

Furthermore, in order to account for the porous character of biological substrates on which the membrane may adhere, such as the cytoskeleton, collagen, or endothellial tissues, we consider walls with arbitrary permeabilities. Such a tunable permeability is also an important feature of membrane stacks in the stratum corneum [4–6]. Our modeling suggests that the spatial organization of the frozen states is controlled by the permeability of the walls. Indeed, the membrane profile exhibits a periodic ordered structure for impermeable walls, and becomes disordered when the wall permeability is increased. This difference can be traced back to the consequences of the permeability on the initial linear instability.

In the following, we start in Section II with a presentation of the hydrodynamic model, and we derive a general evolution equation for a membrane between two walls in the lubrication limit. Then, in Section III, we consider the limits of small and large wall permeabilities. The numerical solution of these limits is discussed in Section IV. These results are discussed in the light of a linear stability analysis in Section V, and of an analysis of the nonlinear steady-states in Section VI. Finally, we summarize our results in the last Section.

II. THE HYDRODYNAMIC MODEL AND THE LUBRICATION REGIME

We consider a membrane in a liquid confined between two parallel walls located in $z = \pm h_0$ (see Fig. 1). We focus on the limit of small Reynolds numbers, and the liquid obeys the Stokes equation:

$$\nabla p_\pm - \mu \Delta \mathbf{v}_\pm = 0, \tag{1}$$

where the subscript $\pm$ indicates the fluid above $(+)$ or below $(-)$ the membrane at $z = h(x,t)$, $p_\pm(x,z)$ is the pressure, μ is the dynamic viscosity, and $\mathbf{v}_\pm = (v_{x\pm}, v_{z\pm})$ is the liquid velocity.

Next, we need to define the boundary conditions at the walls and at the membrane, which separates the upper and lower fluids. At the walls, the tangential component of the velocity vanishes because we assume no-slip conditions, while the normal component depends on wall permeability ν:

$$v_{x\pm}|_{z=\pm h_0} = 0, \tag{2}$$
$$v_{z\pm}|_{z=\pm h_0} = \pm\nu(p_\pm - p_{ext}), \tag{3}$$

where p_{ext} is a constant pressure outside the walls.

Boundary conditions at membrane are more involved. First, following Molecular Dynamics simulations on lipid membranes [28, 29] we also assume no-slip at the membrane,

$$\mathbf{v}_+|_{z=h(x,t)} = \mathbf{v}_-|_{z=h(x,t)}. \tag{4}$$

Then, mechanical equilibrium at the membrane imposes

$$(\mathbf{\Sigma}_+ - \mathbf{\Sigma}_-) \cdot \mathbf{n} = \mathbf{f}, \tag{5}$$

where $\Sigma_{ij} = \mu(\partial_i v_j + \partial_j v_i) - p\delta_{ij}$ is the stress tensor in the fluid, $\mathbf{n}$ is the membrane normal, and $\mathbf{f} = -\delta\mathcal{E}/\delta\mathbf{r}$ is the force exerted by the membrane. This force derives from the energy

$$\mathcal{E} = \int ds \left[\frac{\kappa}{2}C^2 + \mathcal{U}(h)\right], \tag{6}$$

where s is the arclength along the membrane, $C = -\partial_{xx}h/[1+(\partial_x h)^2]^{3/2}$ is the local membrane curvature, κ is the bending rigidity, and $\mathcal{U}(h)$ is the double-well adhesion potential, as shown in the schematic in Fig.1.

Finally, in order to focus on dynamics within a large contact area and to discard boundary effects, we impose periodic boundary conditions along x in a large system of total length L.

The main approximation allowing to obtain the evolution equation for the membrane profile is the small slope approximation $\partial_x h(x,t) \ll 1$, while the height itself can be finite, i.e of the order of h_0. The main lines of the derivation are reported in Appendix A. Using the standard lubrication expansion [30], we obtain

$$\partial_t h = \partial_x \left[-\frac{h_0^3}{24\mu}\left(1 - \frac{h^2}{h_0^2}\right)^3 \partial_x f_z + \frac{3}{4} j \frac{h}{h_0}\left(\frac{h^2}{3h_0^2} - 1\right)\right] + \frac{\nu}{2} f_z, \tag{7}$$

where the membrane force is

$$f_z = -\kappa\partial_x^4 h - \mathcal{U}'(h), \tag{8}$$

and the total liquid flow rate j along x,

$$j = \int_{-h_0}^{h} dz\, u_{x-} + \int_{h}^{+h_0} dz\, u_{x+}, \tag{9}$$

obeys the differential equation

$$-\frac{h_0^3}{3\mu\nu}\partial_{xx} j + j = \frac{1}{2}\frac{h_0^3}{\mu}\frac{h}{h_0}\left(1 - \frac{h^2}{3h_0^2}\right)\partial_x f_z. \tag{10}$$

Two remarks on above equation are in order. First, the equation is nonlocal in space. This nonlocality is seen from the fact that j obeys a time-independent differential equation (10). This constrain comes from the incompressibility of the liquid. Second, the dynamics is variational, i.e. $\partial_t \mathcal{E} \leq 0$, where the energy $\mathcal{E}$ is given by Eq. (6). In the small slope approximation, the curvature is simply $C = -\partial_{xx} h$ and

$$\mathcal{E} = \int dx \left[\frac{\kappa}{2}(\partial_{xx} h)^2 + \mathcal{U}(h)\right]. \tag{11}$$

III. CONSERVED AND NON-CONSERVED LIMITS

We are now going to consider two important limiting cases of Eqs.(7-10), which are better defined using the reduced wall permeability

$$\bar{\nu} = \frac{12\mu\kappa^{1/2}\nu}{h_0^2 \mathcal{U}_0^{1/2}}, \tag{12}$$

where the energy scale $\mathcal{U}_0$ is such that $\mathcal{U}(h) = \mathcal{U}_0 U(H)$, where $U(H)$ is of order one. In the limit of large permeabilities $\bar{\nu} \to \infty$, we obtain

$$\partial_T H = -\partial_X^4 H - U'(H), \qquad \text{[TDGL4]} \tag{13}$$

where $H = h/h_0$, $X = [\mathcal{U}_0/(\kappa h_0^2)]^{1/4} x$, and $T = t\nu\mathcal{U}_0/(2h_0^2)$. In this limit the nonlocality induced by incompressibility vanishes and the resulting equation has a manifest nonconserved character. More precisely, Eq.(13) bears a strong resemblance to the standard Time-Dependent Ginzburg-Landau (TDGL) equation, $\partial_T H = \partial_X^2 H - U'(H)$, which describes phase separation for a non-conserved order parameter [1]. However in Eq.(13), the linear stabilizing term is 4th order instead of being a 2nd order derivative, because it physically derives from bending rigidity rather than from surface tension. For this reason, we denote Eq.(13) as "TDGL4".

In the opposite limit of impermeable walls, $\bar{\nu} = 0$, we obtain

$$\partial_T H = \partial_X \Big\{ (1-H^2)^3 \partial_X [\partial_X^4 H + U'(H)] + JH(\frac{H^2}{3} - 1) \Big\}, \qquad \text{[non-local CH4]} \tag{14}$$

$$J = -\frac{9}{L}\int_0^L \mathrm{d}X\, H \left(1 - \frac{H^2}{3}\right)\partial_X [\partial_X^4 H + U'(H)] \tag{15}$$

where the time variable now exhibits a different normalization $T = \mathcal{U}_0^{3/2} t/(24\mu\kappa^{1/2})$, and $J = 18 j \mu\kappa^{1/4}/(h_0^{3/2}\mathcal{U}_0^{5/4})$. For vanishing permeabilities, the resulting equation is conserved, because the (incompressible) fluid remains confined between the walls. As a consequence, the membrane evolution equation shares similarities with the Cahn-Hilliard (CH) equation $\partial_T H = \partial_{XX}[\partial_X^2 H - U'(H)]$, which describes phase separation for a conserved order parameter [1, 2]. However, there are several differences: (i) The 4th-order derivative in the stabilizing term. This difference was expected, in line with the nonconserved case. (ii) The membrane mobility $\sim (1-H^2)^3$ vanishes as $H \to \pm 1$ due to the well known divergence of viscous dissipation when the membrane approaches the walls [30, 31]. (iii) The non-local effects related to J. The nonlocality is now manifest in the expression of J as an integral over the whole system in Eq. (15). In the following, we denote Eq.(14) as the "non-local CH4" equation.

IV. NUMERICAL STUDY OF MEMBRANE DYNAMICS

As a preamble, before studying the dynamics of Eqs.(13,14) in extended systems, we shall recall the well known dynamics arising from the standard TDGL and CH equations: the profile $H(X,T) \equiv 0$ is unstable and it develops flat regions where H is approximately equal to the values of one or the other minimum of the double-well potential $U(H)$. In the language of our paper, the regions where the membrane lies in a minimum of the potential correspond to adhesion patches. The zones separating two flat regions are called kinks. Within the TDGL or CH models, pairs of kinks collide and annihilate, thereby leading to the decrease of the number of adhesion patches. The typical size λ of these patches therefore exhibits an endless increases in time. This process is called coarsening.

In contrast, the numerical solution of TDGL4 and non-local CH4 does not exhibit any coarsening. In order to support this statement with numerical simulations of the evolution equations, we need to use an explicit form of the two-well potential U. However, in all other sections above and below, the profile of U is kept arbitrary. We have chosen the standard quartic potential

$$U_4(h) = -H_m^2 \frac{H^2}{2} + \frac{H^4}{4}, \tag{16}$$

which exhibits minimums at $H = \pm H_m$, with $H_m < 1$. In the simulations, we use $H_m = 0.9$.

Starting from small random initial conditions we find that after a short transient the membrane forms a frozen pattern, as shown in Fig.2(a,b). In order to gain quantitative insights on the evolution of the system, we define the average wavelength $\langle\lambda\rangle$ as the average distance between two consecutive points obeying $h = 0$ and $\partial_x h > 0$. The plot of $\langle\lambda\rangle$ as a function of time in Fig.2(c) shows

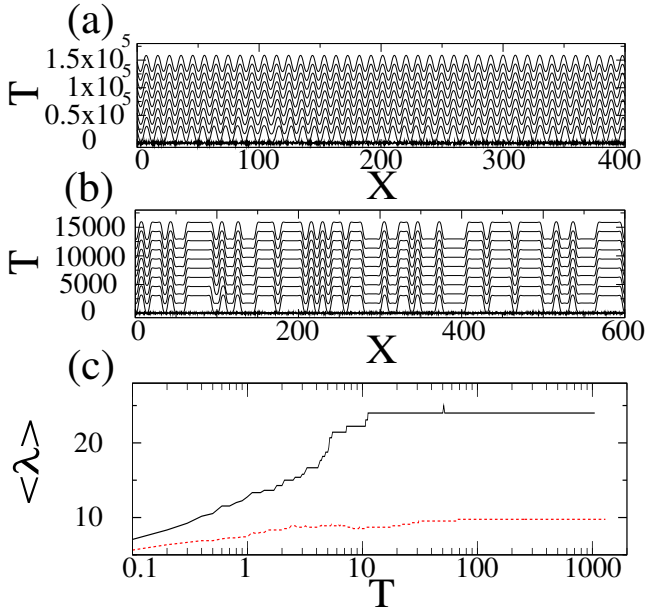

FIG. 2. (Color online) Arrested dynamics and order-disorder transition. (a) Non-permeable case. Frozen ordered patterns obtained from the numerical solution of the CH4 equation, Eq.(14). (b) Permeable case. Frozen disordered patterns obtained from the numerical solution of the TDGL4 equation, Eq.(13). In (a,b) the vertical scale is increased by a factor ~ 10 for a better visibility of the membrane morhology. (c) Saturation of the spatially averaged wavelength $\langle\lambda\rangle$ as a function of time. The black solid line and the red dotted line correspond to TDGL4 Eq.(13) and CH4 Eq.(14) respectively.

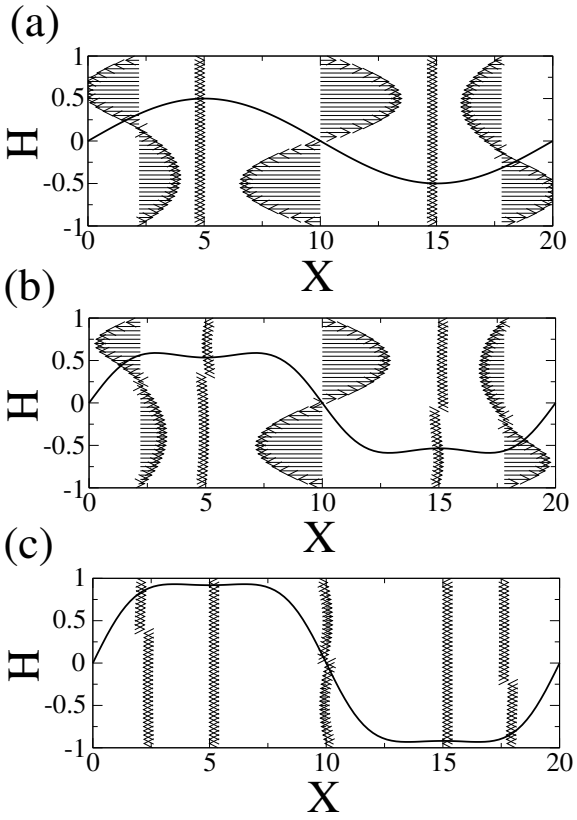

FIG. 3. Snapshots of hydrodynamics flows and membrane profile during the dynamics in the conserved case Eq. (14). Horizontal arrows represent the hydrodynamic flow. (a) The initial membrane profile is a single period of a sinusoid. (b) Intermediate times. (c) The final membrane profile exhibits plateaus separated by kinks.

a clear saturation after a time of the order of 10 to 30 in reduced units. Furthermore, while the frozen pattern is ordered and periodic in the presence of impermeable walls, it is clearly disordered for permeable walls. We stress that we have observed no difference between the numerical solution of non-local CH4 and Eq.(14) with $J = 0$, simply denoted as CH4 in the following.

As a first remark on the numerical results, we indicate that simulations with other forms of the double-well potential U have shown no qualitative difference in the results. However, quantitative changes can be observed. As an important example, when $H_m \to 1$, the conserved dynamics Eq. (14) slow down considerably in the late stages because the mobility term $(1-H^2)^3$ is small in the plateaus between the kinks where H is close to H_m. In constrast, there is no similar effect in the non-conserved case Eq. (13).

A second remark: the final ordered state obtained in Fig. 2(a) for CH4 does not evolve further if used as initial configuration for TDGL4. And vice versa, the final disordered state of TDGL4 in Fig. 2(b) does not evolve under CH4 dynamics: this is exactly what we observe from the numerical solution of the equations. This leads to two important conclusions: (i) the conseved and non-conserved equation seem to share the same stable steady-states; (ii) even though distinct ordered and disordered states are robustly observed with random initial conditions, the final state may also depend on peculiar initial conditions.

Third remark, once we have the dynamical profile of the membrane, we also have access to the full hydrodynamic flow during the evolution of the membrane using Eq. (A1). As an example, we show the flow around an initially sinusoidal membrane profile in the conserved dynamics in Fig. 3.

Finally, we observed that the normalized slopes remain finite in all simulations, i.e. $\max|\partial_X H| \sim 1$ at all times. As a consequence, the small slope approximation $\partial_x h \ll 1$ is self-consistent: if this assumption is true initially, it remains true for all times.

In the next sections, we propose some analytical results which confirm the scenario proposed by the numerical solution of the membrane dynamics.

V. LINEAR STABILITY ANALYSIS OF FLAT MEMBRANES

As a summary of results so far, Fig. 2 highlights two important features: (i) absence of coarsening and (ii) a frozen state which is disordered for $\bar{\nu} = \infty$ (TDGL4) and ordered for $\bar{\nu} = 0$ (non-local CH4 or CH4). The latter feature can be traced back to the different behaviors of the two equations with respect to small perturbations around the average height $\bar{H}$. Inserting $H(X,T) = \bar{H} + \delta H e^{i\omega T + iqX}$ with $\delta H \ll 1$ in Eq.(13) we obtain to linear order the dispersion relation for TDGL4

$$i\omega = -U''(\bar{H}) - q^4. \qquad \text{[TDGL4]} \qquad (17)$$

As a remark, in the limit of permeable walls and when $U'(\bar{H}) \neq 0$, the average height $\bar{H}$ depends on time. Hence, strictly speaking the dynamical evolution of the Fourier modes is not exponential. However, the dispersion relation still provides a qualitative description of the unstable modes at short times for $\bar{H} \neq 0$. In addition, the linear stability analysis also provides a strictly valid description for the case $\bar{H} = 0$ studied in the numerical simulations above, because $\bar{H}$ is constant in this case.

In contrast, $\bar{H}$ is always constant in the conserved equations, and the exponential time-dependence of the perturbation amplitude is strictly valid in this case. The linear dispersion relation for non-local CH4 or CH4 (i.e. with or without the J term) provides the same dispersion relation

$$i\omega = (1-\bar{H}^2)^3 q^2 [-U''(\bar{H}) - q^4]. \qquad \text{[CH4]} \qquad (18)$$

Both for permeable and impermeable walls, an instability, indicated by $i\omega > 0$, appears at long wavelength when $U''(\bar{H}) < 0$. As seen in Fig. 4(a), while TDGL4 destabilizes all long wavelength modes with the same growth rate $i\omega \sim -U''(\bar{H})$ at $q \to 0$, CH4 exhibits a special mode at $q_u = [-U''(\bar{H})/3]^{1/4}$ for which the growth rate is maximum. Hence, we expect initially a disordered pattern with many wavelengths in the limit of permeable walls, and an ordered pattern with a single wavelength $\lambda_u = 2\pi/q_u$ in the limit of impermeable walls. In Fig. 4(b), we have plotted the histogram of λ, the double of the distances between the zeros of H in the frozen state when starting from random initial conditions. The quantity λ is a measure of the local wavelength. For non-local (and local) CH4, the linear instability produces an initial periodic pattern with a single wavelength $\lambda_u \approx 2\pi/q_u$, while for TDGL4, we indeed obtain a wide distribution of distances.

VI. STABILITY OF PERIODIC STEADY-STATES

Although linear analysis indicates when we should expect order or disorder, it does not provide insights about why the dynamics should freeze, as observed in the simulations. In order to gain insights on this subject we study the stability of fully nonlinear periodic steady-states. The steady-states of the TDGL and CH equations, solutions of $\partial_X^2 H - U'(H) = 0$, are known to be periodic with a single maximum in each period. For each wavelength λ, there is a unique steady-state. For Eq.(7), and all its special limits TDGL4, CH4, and non-local CH4, the steady-states obey

$$\partial_X^4 H + U'(H) = 0. \qquad (19)$$

It is actually known that Eq.(19) exhibits not only periodic solutions with several maximums per period, but also an infinite number of non-periodic solutions (chaotic along x) [32]. However, we shall show in the following that the study of periodic steady-states provides a reasonable description of the nonlinear dynamics.

For this purpose, consider a family of periodic steady-states H_λ parametrized by the wavelength λ. We wish to study the stability of a uniform periodic steady-state under long-wavelength variations of λ. Defining a macroscopic variable $\tilde{X}$ at scales much larger than λ, the total energy may be approximated as the integral on the slow variable $\tilde{X}$ of the energy density in one period

$$\mathcal{E} = \int \frac{d\tilde{X}}{\lambda(\tilde{X})} \int_0^{\lambda(\tilde{X})} dX e_{\lambda(\tilde{X})}(X) \qquad (20)$$

where

$$e_{\lambda(\tilde{X})}(X) = [\partial_{XX} H_{\lambda(\tilde{X})}(X)]^2/2 + U(H_{\lambda(\tilde{X})}(X)) \qquad (21)$$

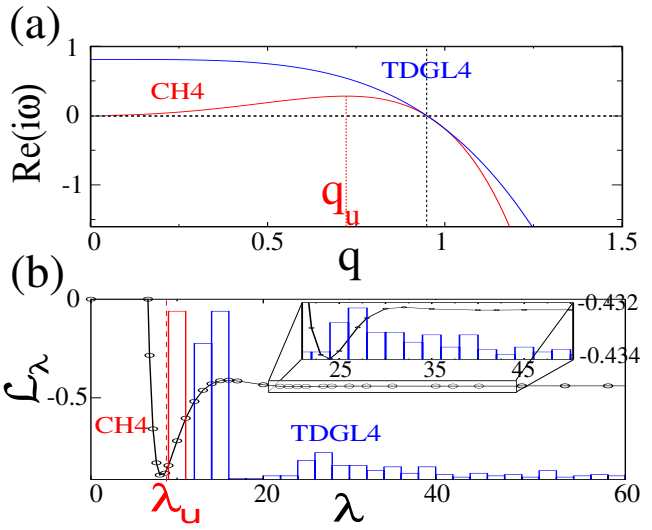

FIG. 4. (Color online) (a) Linear dispersion relation. (b) Histogram of the distances between kinks. The solid line reports the value of minus the total curvature energy in one steady-state period $\mathcal{L}_\lambda = -\int_0^\lambda (\partial_{XX} H_\lambda(X))^2$, obtained numerically from the periodic double-kink solution shown in Fig. 5. As discussed in Sec. VI, $\mathcal{L}_\lambda$ controls the stability of the steady-states. The dashed line corresponds to the approximate expression of Eq.(26) with $\mathcal{L}_0 = -0.43225$.

is the local energy density. We then consider a small perturbation around the average wavelength $\lambda(\tilde{X}) = \bar{\lambda} + \delta\lambda(\tilde{X})$. Since $\delta\lambda(\tilde{X})$ is small, the total number $\mathcal{N} = \int d\tilde{X}/\lambda(\tilde{X})$ of steady-state periods in the system is constant, i.e. $\delta\mathcal{N} = 0$, leading to the relation

$$\lambda \int d\tilde{X}\delta\lambda(\tilde{X}) \approx \int d\tilde{X}\delta\lambda(\tilde{X})^2 + O(\delta\lambda(\tilde{X})^3). \quad (22)$$

Using this relation and Eq.(19), one may then calculate the variation of total energy

$$\delta\mathcal{E} = \frac{\partial_{\bar{\lambda}}\mathcal{L}_{\bar{\lambda}}}{\bar{\lambda}^2} \int d\tilde{X}[\delta\lambda(\tilde{X})]^2 + O([\delta\lambda(\tilde{X})]^3), \quad (23)$$

where

$$\mathcal{L}_\lambda = -\int_0^\lambda (\partial_{XX} H_\lambda(X))^2. \quad (24)$$

Since we know that the dynamics always decreases $\mathcal{E}$, i.e. $\partial_t\mathcal{E} \leq 0$, the perturbation amplitude $\int d\tilde{X}[\delta\lambda(\tilde{X})]^2$ must decrease if $\partial_\lambda\mathcal{L}_\lambda > 0$, and must increase if $\partial_\lambda\mathcal{L}_\lambda < 0$. Hence, the periodic steady-state of wavelength $\bar{\lambda}$ is stable if $\partial_\lambda\mathcal{L}_\lambda > 0$ and unstable if $\partial_\lambda\mathcal{L}_\lambda < 0$. This criterion shows that the stability depends only on the energy $\mathcal{E}$, and is independent of the precise kinetics. This criterion based on the energy is valid for the general Eq.(7), and its various specific limits (TDGL4, non-local CH4, or CH4).

We use a branch of steady-state solutions which provide the double-kink solution shown in Fig. 5 at long wavelengths to calculate $\mathcal{L}_\lambda$. Hereafter, we define a kink as a localized region of the membrane profile going from $\mp H_m$ for $x \to -\infty$ to $\pm H_m$ for $x \to +\infty$. This branch can for example be obtained from the relaxation with TDGL4 of an initial condition composed of a double kink with tanh profiles. In Fig. 4(b), we have plotted $\mathcal{L}_\lambda$ from this steady-state branch. We see that $\partial_\lambda\mathcal{L}_\lambda > 0$ for the most unstable wavelength of the CH4 or non-local CH4 equations, $\lambda = \lambda_u$. Hence, our stability criterion explains that the periodic steady-state reached by the dynamics via the linear instabilty of CH4 or non-local CH4 is frozen.

The case of the TDGL4 equation is more delicate to analyze because we start with a disordered state as discussed earlier. However, we see peaks in the histogram of Fig. 4(b) in the stable regions with $\partial_\lambda\mathcal{L}_\lambda > 0$, and valleys when $\partial_\lambda\mathcal{L}_\lambda < 0$. This is in agreement with a scenario where pairs of zeros separated by a distance corresponding to $\partial_\lambda\mathcal{L}_\lambda < 0$ are unstable, and the whole system finally recombines into a configuration where the distance between the zeros are in the stable regions. However, note that for large distances, no reorganization is obtained within the simulation time.

A striking feature of the stability criterion in Fig. 4(b) is its oscillatory character. These oscillations originate in the fourth order derivative in Eq.(19), which induces an oscillatory membrane profile in the vicinity of the kinks, as shown in Fig. 5. Expanding Eq.(19) in the vicinity of the minima of potential wells at $H = H_m$ for $X > X_k$,

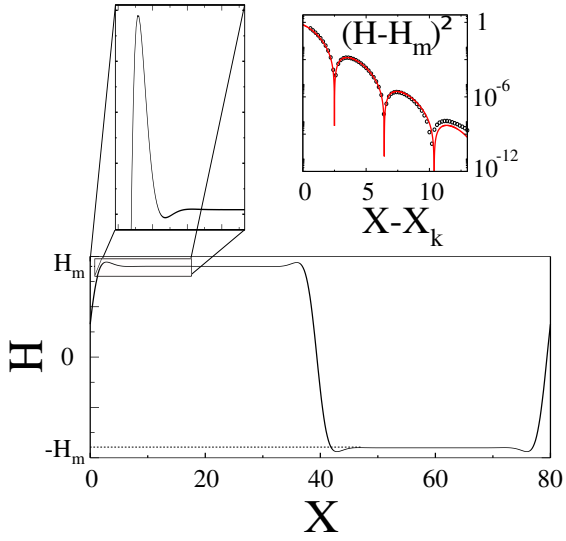

FIG. 5. (Color online) Periodic double-kink steady-state profile. The insets show a zoom on an oscillatory kink tail, and the oscillations of $(H - H_m)^2$ in log scale away from a kink. The transient dynamics leading to this periodic steady-state is shown in Fig. 3.

where X_k is the position of the kink, we find an explicit expression for the kink tails $H(X) = H_m + R(X - X_k)$, with

$$R(\ell) = A\cos\left(\frac{\ell U_m''^{1/4}}{2^{1/2}} + \alpha\right)\exp\left[-\frac{\ell U_m''^{1/4}}{2^{1/2}}\right]. \quad (25)$$

Here $U_m'' = U''(H_m)$, and $A > 0$ and α are constants depending on details of the potential profile. Since we do not have an analytical expression for the full kink profile, the exact values of A and α are unknown and depend on the precise profile of U. However, a simple argument provides an approximate value. Indeed, assuming that the profile $H(X) = H_m + R(X - X_k)$ with R given in Eq.(25) extends beyond its domain of validity up to the center of the kink where $X \to X_k$, we request the continuity of H at $X = X_k$ up to the third derivative, leading to $H(X_k) = 0$, and $\partial_{XX}H(X_k) = 0$. As a consequence of these assumptions, one finds $A = H_m$, and $\alpha = \pi$. For the specific case of the quartic potential $\mathcal{U}(H) = \mathcal{U}_4(H)$ with $H_m = 0.9$, these constants can be determined numerically by fitting the profile of the tail of an isolated kink with Eq.(25), as shown in the inset of Fig. 5. We then find values which are close to the approximate predictions: $A = 0.87$, and $\alpha = 2.72$.

For large distances between the kinks $\lambda \gg 1$, the behavior of $\mathcal{L}_\lambda$ is actually dominated by the asymptotic tails of the kinks, and substituting Eq.(25) into Eq.(24), we find to leading order:

$$\mathcal{L}_\lambda \approx \mathcal{L}_0 + A^2 U_m''\lambda\cos\left(\frac{\lambda U_m''^{1/4}}{2^{3/2}} + 2\alpha\right)\exp\left[-\frac{\lambda U_m''^{1/4}}{2^{3/2}}\right], \quad (26)$$

where $\mathcal{L}_0$ is an unknown constant. This expression is in good agreement with the value of $\mathcal{L}$ obtained from the numerical profile of the steady-state branch, as shown in Fig. 4(b). As discussed above, the stability criterion is related to the sign of

$$\partial_\lambda \mathcal{L}_\lambda \approx -\frac{1}{2} A^2 {U''_m}^{5/4} \lambda \cos\left(\frac{\lambda {U''_m}^{1/4}}{2^{3/2}} + 2\alpha - \frac{\pi}{4}\right) \times \exp\left[-\frac{\lambda {U''_m}^{1/4}}{2^{3/2}}\right]. \quad (27)$$

This expression shows explicitly the oscillatory character of the stability as a function of the distance between kinks.

VII. FINAL CONSIDERATIONS

As a summary, we have derived a nonlinear and nonlocal dynamical equation, see Eq. (7), from a hydrodynamic model for a membrane separating two incompressible fluids and confined between two rigid walls, see Fig. 1. This equation has been studied numerically and analytically in the limit of large wall permeability ($\bar{\nu} \to \infty$), leading to the nonconserved Eq. (13), and in the limit of vanishing wall permeability ($\bar{\nu} \to 0$), leading to the conserved Eq. (14).

The bending rigidity of the membrane induces a novel class of behavior. Indeed both for small and large $\bar{\nu}$, the system evolves towards a frozen state, the details of which depend on the initial state. Generic, random initial configurations lead to a disordered state for large $\bar{\nu}$ (conserved case) and to an ordered periodic state for vanishing $\bar{\nu}$ (nonconserved case). The non-local character of the dynamics appears to be either vanishing ($\bar{\nu} \to \infty$) or irrelevant ($\bar{\nu} \to 0$).

The orders of magnitude of the lengthscales and timescales of the patterns discussed in this paper should be observable experimentally. Indeed, following Ref. [10], we consider as an example an attractive Van der Waals interaction and the hydration repulsion between a membrane and a substrate. Using a gap $2h_0 = 20$nm with $\bar{h} = 0$, the most unstable wavelength in the case of impermeable walls (non-local CH4) is $\lambda_u = 2\pi/q_u \approx 350$nm and $t_u \approx 1 \times 10^{-2} s$.

Besides the need of generalization of our approach to two-dimensional membranes, one important perspective of our work is to test the robustness of the frozen states with respect to various additional physical ingredients. As an example, a membrane tension σ can be added to the model, leading to an additional stabilizing term $\sigma \partial_{xx} h$ in the expression of the membrane force Eq.(8). For large enough tensions, the oscillations in the kink tails disappear. As expected, the dynamics for large tensions is similar to that of TDGL or CH, with logarithmic coarsening. From a simple dimensional analysis, this behavior is expected for tensions larger than $\sigma_c \sim (\mathcal{U}_0 \kappa)^{1/2}/h_0$, with a prefactor of the order of 1. A detailed account of this transition confirms this prediction, and will be provided elsewhere [33]. Using once again numbers from Ref.[10], we find $\sigma_c \sim 10^{-2}\mathrm{J.m}^{-2}$. Values for the tension of supported membranes extracted from experiments are in the range $\sigma \approx 10^{-5} - 10^{-3}$J from Refs. 10 and 34. As a consequence the tensions observed in supported membranes are much smaller than σ_c, and their effects should be negligible. However, the area increase (or decrease) in the kinks during the formation (or annihilation) of adhesion patches could also lead to additional tension effects.

Other ingredients, such as potential asymmetry and noise could also destabilize the frozen states reported here. We plan to report along these lines in the near future.

ACKNOWLEDGMENTS

We acknowledge support from Biolub grant ANR-12-BS04-0008 (TLG,PP,OPL), and from INFN (OPL).

Appendix A: Lubrication limit

Here we provide the main lines of the derivation of an evolution equation for the membrane in the lubrication limit. We start with a slightly more general description as compared to the one discussed in the main text. Indeed, we describe the hydrodyanmics with the full Navier-Stokes equations, including inertial effects. Consider a fluid in two dimensions x, z:

$$\rho(\partial_t v_x + v_x \partial_x v_x + v_z \partial_z v_x) = -\partial_x p + \mu \nabla^2 v_x,$$
$$\rho(\partial_t v_z + v_x \partial_x v_z + v_z \partial_z v_z) = -\partial_z p + \mu \nabla^2 v_z,$$

where ρ is the density of the fluid, and the other notations are defined in the main text.

We define a small parameter $\epsilon = h_0/\ell \ll 1$ where ℓ is the typical extent of the adhesion patches along x. We may then define dimensionless variables $X = \epsilon x/h_0$, $Z = z/h_0$. Following the usual procedure for the lubrication expansion [30], we also use normalized velocities $V_X = v_x/v_0$ and $V_Z = v_z/(\epsilon v_0)$, and pressure $P = \epsilon h_0/(\mu v_0)$, where v_0 is the typical fluid velocity. With these new variables, we obtain

$$\epsilon\,\mathrm{Re}(\partial_T V_X + V_X \partial_X V_X + V_Z \partial_Z V_X) = -\partial_X P + \partial_Z^2 V_X + \epsilon^2 \partial_X^2 V_X,$$
$$\epsilon^3\,\mathrm{Re}(\partial_T V_Z + V_X \partial_X V_Z + V_Z \partial_Z V_Z) = -\partial_Z P + \epsilon^2(\partial_Z^2 V_Z + \epsilon^2 \partial_X^2 V_Z),$$

where $\mathrm{Re} = \rho v_0 h_0/\mu$ is the Reynolds number. Assuming that Re is at most of order one, and in the lubrication approximation $\epsilon \to 0$, we obtain to leading order $-\partial_X P + \partial_Z^2 V_X = 0$, and $-\partial_Z P = 0$. As a consequence P depends

only on X, and V_X exhibits a simple quadratic form

$$V_X = \frac{Z^2}{2}\partial_X P + AZ + B, \tag{A1}$$

where P, A and B are 3 unknown functions of X which do not depend on Z. Since the fluid may have different velocity profiles above and below the membrane, we obtain 6 unknown functions of X. It is convenient to define the total flow rate J obeying

$$J = \int_{-1}^{1} dZ\, V_X \tag{A2}$$

as a seventh unknown function of X.

These seven unknown functions of X are obtained using the boundary conditions at the wall and at the membrane. The no-slip conditions at the walls and at the membrane, Eqs.(2,4), provide three equations. Then, mechanical equilibrium at the membrane, Eq.(5), leads to two additional equations. Hence, we have five equations:

$$V_{X+}|_{Z=1} = 0, \tag{A3}$$
$$V_{X-}|_{Z=-1} = 0, \tag{A4}$$
$$V_{X+}|_{Z=H} = V_{X-}|_{Z=H}, \tag{A5}$$
$$P_+ - P_- = F_Z, \tag{A6}$$
$$\partial_Z V_{X+}|_{Z=H} = \partial_Z V_{X-}|_{Z=H}. \tag{A7}$$

Mass conservation and the wall permeability condition, Eq.(3), provide two other equations:

$$\partial_X J = -\tilde{\nu}(P_+ + P_- - 2P_{ext}), \tag{A8}$$
$$\partial_T H = -\frac{1}{2}\partial_X(J_- - J_+) + \frac{\tilde{\nu}}{2}(P_+ - P_-), \tag{A9}$$

where $\tilde{\nu} = \nu\mu\ell^2 h_0^{-3}$, and the upper and lower liquid flow rates are defined as

$$J_- = \int_{-1}^{H} dZ\, V_X, \tag{A10}$$
$$J_+ = \int_{H}^{1} dZ\, V_X. \tag{A11}$$

Using the seven equations (A2-A8) provides the seven unknowns. Inserting these expressions in Eq.(A9) and going back to physical variables leads to the evolution equation of the membrane, Eq.(7).

[1] P. C. Hohenberg and B. I. Halperin, Rev. Mod. Phys. **49**, 435 (1977).
[2] J. W. Cahn and J. E. Hilliard, The Journal of Chemical Physics **28**, 258 (1958).
[3] D. Boal, Mechanics of the cell (Cambridge University Press, 2002).
[4] European Journal of Pharmaceutical Sciences **50**, 638 (2013), (Trans)dermal drug delivery: Emerging trends to study and overcome the skin barrier.
[5] C. Das, P. D. Olmsted, and M. G. Noro, Soft Matter **5**, 4549 (2009).
[6] C. Das, M. G. Noro, and P. D. Olmsted, Biophys. Journal **97**, 1951 (2009).
[7] C. Das, M. G. Noro, and P. D. Olmsted, Biointerphases **7**, 57 (2012).
[8] M. S. Jablin, M. Zhernenkov, B. P. Toperverg, M. Dubey, H. L. Smith, A. Vidyasagar, R. Toomey, A. J. Hurd, and J. Majewski, Phys. Rev. Lett. **106**, 138101 (2011).
[9] J. Daillant, E. Bellet-Amalric, A. Braslau, T. Charitat, G. Fragneto, F. Graner, S. Mora, F. Rieutord, and B. Stidder, Proceedings of the National Academy of Sciences of the United States of America **102**, 11639 (2005).
[10] P. S. Swain and D. Andelman, Phys. Rev. E **63**, 051911 (2001).
[11] D. Zuckerman and R. Bruinsma, Phys. Rev. Lett. **74**, 3900 (1995).
[12] R. Lipowsky, Phys. Rev. Lett. **77**, 1652 (1996).
[13] T. Speck and R. L. C. Vink, Phys. Rev. E **86**, 031923 (2012).
[14] A. Hemmerle, L. Malaquin, T. Charitat, S. Lecuyer, G. Fragneto, and J. Daillant, **109**, 19938 (2012).
[15] W. Helfrich, Z. Naturforsch. A **33**, 305 (1978).
[16] L. B. Freund, **110**, 2047 (2013).
[17] T. Auth and G. Gompper, Phys. Rev. E **88**, 010701 (2013).
[18] T. R. Weikl, M. Asfaw, H. Krobath, B. Rozycki, and R. Lipowsky, Soft Matter **5**, 3213 (2009).
[19] R. Bruinsma, A. Behrisch, and E. Sackmann, Phys. Rev. E **61**, 4253 (2000).
[20] K. Sengupta and L. Limozin, Phys. Rev. Lett. **104**, 088101 (2010).
[21] P. B. Canham, J. Theor. Biol **26**, 61 (1970).
[22] W. Helfrich, Z. Naturforsch. **28c**, 693 (1973).
[23] B. G. Lorz, A.-S. Smith, C. Gege, and E. Sackmann, Langmuir **23**, 12293 (2007).
[24] E. Reister-Gottfried, K. Sengupta, B. Lorz, E. Sackmann, U. Seifert, and A.-S. c. v. Smith, Phys. Rev. Lett. **101**, 208103 (2008).
[25] T. Bihr, U. Seifert, and A.-S. c. v. Smith, Phys. Rev. Lett. **109**, 258101 (2012).
[26] A. Kusumi, C. Nakada, K. Ritchie, K. Murase, K. Suzuki, H. Murakoshi, R. S. Kasai, J. Kondo, and T. Fujiwara, Annual Review of Biophysics and Biomolecular Structure **34**, 351 (2005), pMID: 15869394.
[27] H. Delanoë-Ayari, P. Lenz, J. Brevier, M. Weidenhaupt, M. Vallade, D. Gulino, J. F. Joanny, and D. Riveline, Phys. Rev. Lett. **93**, 108102 (2004).
[28] T. J. Mueller and F. Mueller-Plathe, ChemPhysChem **10**, 2305 (2009).
[29] Y. von Hansen, S. Gekle, and R. R. Netz, Phys. Rev.

Lett. **111**, 118103 (2013).
[30] A. Oron, S. H. Davis, and S. G. Bankoff, Rev. Mod. Phys. **69**, 931 (1997).
[31] J. Happel and H. Brenner, Low Reynolds Number Hydrodynamics (Kluwer, 1983).
[32] L. Peletier and W. Troy, Spatial Patterns (Birkhauser Boston, 2001).
[33] T. Le Goff, P. Politi, and O. Pierre-Louis, unpublished (2014).
[34] L. Malaquin, T. T. Charitat, and J. Daillant, The European Physical J E **31**, 285 (2010).